

1 A Simple Framework for Calibrating 2 Hydraulic Flood Inundation Models using 3 Crowd-sourced Water Levels

4 Antara Dasgupta^{1,2,3*§}, Stefania Grimaldi³, RAAJ Ramsankaran², Valentijn R.N. Pauwels³,
5 and Jeffrey P. Walker³

6 ¹ IITB-Monash Research Academy, Mumbai, India.

7 ² Department of Civil Engineering, Indian Institute of Technology Bombay, Mumbai, India.

8 ³ Department of Civil Engineering, Monash University, Clayton, VIC, Australia.

9 [§] Now at Remote Sensing Working Group, Institute of Informatics, University of
10 Osnabrück, Germany (antara.dasgupta@uos.de).

11 *Under review (#2 – First Revision) Journal of Hydrology © Elsevier*

12 Twitter handle of lead author: @ant_dasgupta

13 Author email addresses:

14 Stefania Grimaldi: ste.grimaldi.i@gmail.com

15 RAAJ Ramsankaran: ramsankaran@civil.iitb.ac.in

16 Valentijn Pauwels: valentijn.Pauwels@monash.edu

17 Jeffrey Walker: jeff.walker@monash.edu

18 **NOTE: THIS PAPER IS A NON-PEER REVIEWED PREPRINT SUBMITTED TO**
19 **EarthArXiv.**

20 A Simple Framework for Calibrating 21 Hydraulic Flood Inundation Models using 22 Crowd-sourced Water Levels

23 Antara Dasgupta, Stefania Grimaldi, RAAJ Ramsankaran, Valentijn R.N. Pauwels, and
24 Jeffrey P. Walker

25 **Abstract:** Floods are the most commonly occurring natural disaster, with the Centre for
26 Research on the Epidemiology of Disasters 2021 report on “The Non-COVID Year in
27 Disasters” estimating economic losses worth over USD 51 million and over 6000 fatalities in
28 2020. The hydrodynamic models which are used for flood forecasting need to be evaluated and
29 constrained using observations of water depth and extent. While remotely sensed estimates of
30 these variables have already facilitated model evaluation, citizen sensing is emerging as a
31 popular technique to complement real-time flood observations. However, its value for
32 hydraulic model evaluation has not yet been demonstrated. This paper tests the use of crowd-
33 sourced flood observations to quantitatively assess model performance for the first time. The
34 observation set used for performance assessment consists of 32 distributed high water marks
35 and wrack marks provided by the Clarence Valley Council for the 2013 flood event, whose
36 timings of acquisition were unknown. Assuming that these provide information on the peak
37 flow, maximum simulated water levels were compared at observation locations, to calibrate
38 the channel roughness for the hydraulic model LISFLOOD-FP. For each realization of the
39 model, absolute and relative simulation errors were quantified through the root mean squared
40 error (RMSE) and the mean percentage difference (MPD). Similar information was extracted

41 from 11 hydrometric gauges along the Clarence River and used to constrain the roughness
42 parameter. The calibrated parameter values were identical for both data types and a mean
43 RMSE value of ~50 cm for peak flow simulation was obtained across all gauges. Results
44 indicate that integrating uncertain flood observations from crowd-sourcing can indeed generate
45 a useful dataset for hydraulic model calibration in ungauged catchments, despite the lack of
46 associated timing information.

47 **Keywords:** LISFLOOD-FP, hydrodynamic modelling, crowd-sourcing, sensitivity analysis,
48 model evaluation.

49 **1 Introduction**

50 Hydraulic models have traditionally been calibrated with observations of channel flow
51 and water depth, measured by hydrometric river gauges (Domeneghetti et al. 2014). For pluvial
52 events where the flooding could be disconnected from the channel, gauges within the channel
53 cannot provide useful information (Assumpção et al. 2018). Remote sensing (RS) forms part
54 of the solution, however, hurdles such as cost and frequency of acquisition have to be fully
55 addressed to enable routine use of RS data (Grimaldi et al. 2016). Moreover, the definition of
56 an optimal RS-derived product (water level/flood extent) including resolution and acquisition
57 time, as well as the definition of appropriate ways to evaluate and account for RS-derived data
58 uncertainty, still remain a challenge and are active areas of research.

59 As a complement to RS or where RS data are not available, crowd-sourced data can be
60 utilized to supplement flood information (Annis & Nardi 2019). For example, for flash floods
61 or fast moving floods in small catchments, the latency between satellite tasking, acquisition,
62 and data delivery for commercial satellites, or the revisit cycles for public satellites (Lopez et
63 al. 2020), could prove to be prohibitive, resulting in the flood wave having receded before it
64 can be imaged (See 2019). Consequently, novel sources of low-cost data which can be acquired

65 frequently and in abundance are needed. Citizen science (including citizen participation up to
66 the scientist level) or crowd-sourcing (distributing a task among many agents), is an emerging
67 concept in which citizens monitor the environment around them (See et al. 2016). In recent
68 years, citizen science has provided distributed data on a variety of hydraulic variables,
69 including water level (Kutija et al. 2014), flow velocity (Le Boursicaud et al. 2016; Le Coz et
70 al. 2016), flood extent (Schnebele et al. 2014), topography (Shaad et al. 2016), and land-use
71 land-cover (See et al. 2016). Furthermore, the extraction of water levels from crowd-sourced
72 images of flooding from social media has also been automated successfully to a large extent,
73 allowing practitioners to access often large databases of such observations previously
74 inaccessible (e.g., Fohringer et al. 2015; Chaudhary et al. 2019; Chaudhary et al. 2020). As
75 Nardi et al. (2021) assert in their transdisciplinary conceptual framework for citizen science in
76 hydrology, the ubiquity of such data demands the development of novel approaches to leverage
77 this information and reduce flood model uncertainties.

78 On reviewing the potential of citizen science for flood modelling, Assumpção et al.
79 (2018) found a clear lack of appropriate techniques to utilize these data for model calibration
80 and validation. The few studies which have examined the impact of including crowd-sourced
81 water level data, have either used qualitative approaches (Kutija et al. 2014; Yu et al. 2016) or
82 focused on hydrological model validation with synthetic observations (Mazzoleni et al. 2015;
83 Mazzoleni et al. 2018). Approaches to utilize crowd-sourced observations of water level for
84 effective model parameterization still need to be developed (Paul et al. 2018). This study
85 demonstrates for the first time the quantitative use of crowd-sourced flood observations to
86 parameterize a hydraulic model. Here, crowd-sourced observations of floodplain water levels
87 were used to identify a uniform channel roughness. In simple terms, the channel roughness
88 quantifies the resistance to the flow of water exerted by the channel per unit area, typically
89 determined by the river bed vegetation type and density.

90 The primary objective of this study was to develop a simple framework to utilize water
91 level observations from crowd-sourced data for model calibration. Calibration here implies
92 fine-tuning the model parameters so that the simulations optimally fit the observations
93 (Assumpção et al. 2018). The parameter values identified using crowd-sourced data were then
94 compared with those derived from gauges, allowing verification of the parameter choice guided
95 by crowd-sourced observations. Finally, flood extent from the calibrated model was validated
96 against an independent optical remote sensing image acquired during the receding limb, i.e. the
97 post-peak phase when the river water levels have reduced and the excess water has been
98 discharged into the floodplain as overland flow.

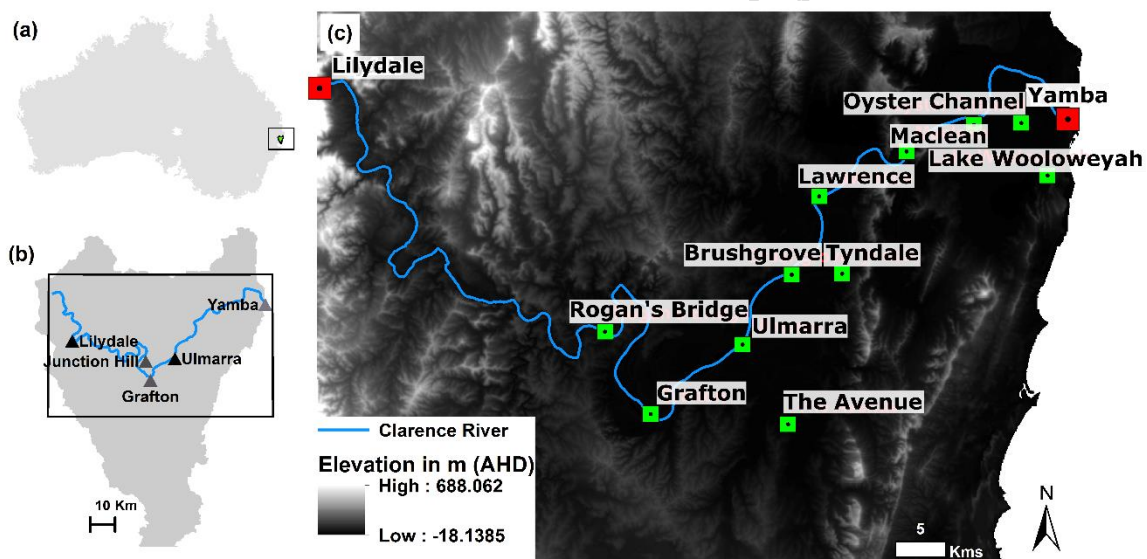


Figure 1. Geographical location of the Clarence Catchment, Australia shown in (a), with the Clarence River and nearby towns marked with respect to the Clarence River Catchment in (b). The extent of the model domain from Lilydale to Yamba is shown in (c), with model boundary conditions marked in red squares while gauge locations are represented by green squares. The LiDAR DEM made available by Geoscience Australia is displayed as the base layer.

99 **2 Study Area**

100 The Clarence Catchment is situated in the far north coast of New South Wales. It is one
101 of the largest river systems on the South-Eastern coast of Australia (Figure 1), with a net
102 drainage area of about 22,700 sq. kms. The Clarence Valley extends from 28°30' S to 30°25' S
103 latitude and 152°4' E to 153°21' E longitude. The main stem of the river is approximately 394
104 km long and occupies the southern part of the Clarence-Moreton Basin in north-eastern New
105 South Wales. The study reach from Lilydale to Yamba is approximately 164 km in length. The
106 land cover of the Clarence region is primarily dominated by grassland vegetation and
107 agriculture, with some urban settlements around Grafton, Ulmarra, Maclean, and Yamba. The
108 mean annual rainfall for the basin is 1,111 mm and mean annual actual evapotranspiration is
109 854 mm.

110 The Clarence River is perennial with a mean annual flow of ~5,727 GL and a runoff
111 coefficient of about 0.23 (NLWRA 2000). There have been 73 major and moderate flood events
112 since 1839, with the most recent major events recorded in 2022, 2021, 2013, and 2011 (Huxley
113 & Beaman 2014). The largest flood on record occurred in 2013, which reached water levels of
114 8.09 m Australian Height Datum (AHD) at Grafton, Prince Street Gauge (Huxley & Beaman
115 2014). Floods in this catchment move fast, resulting in a flashy catchment response, i.e. the
116 time lag between precipitation excesses and the associated inundation is rather short
117 (Rogencamp 2004). For example, in 2011, the flood peak travelled from Lilydale to Yamba in
118 less than 30 h (Grimaldi et al. 2018). Low-intensity, long-duration rainfall events are the
119 dominant cause of flooding in the area, closely followed by the back propagation of ocean
120 storm tides which control inundation dynamics as far upstream as Maclean (Ye et al. 1997).
121 The catchment is characterized by flow velocities ranging from 2-5 m/s in the channel and the
122 levee system, to almost zero in the backwaters (Sinclair Knight Merz & Roads and Traffic

123 Authority of NSW 2011). Extensive levee walls have been constructed to protect Grafton,
124 Ulmarra, and Maclean from flooding (Rogencamp 2004).

125 **3 Data Description**

126 The Clarence Valley Council provided field data in the form of photographs of wrack
127 marks (debris deposited at the flood edge) and water marks (staining on the side of structures
128 within the flooded area) some of which are available online^{1,2,3,4}. These photographs were
129 collected and interpreted visually by the council experts immediately after the 2013 event, and
130 were provided as 32 water level observations whose timing of acquisition was unknown.
131 Further information on the collection of the images is unfortunately unavailable to the authors
132 or even to the council, due to personnel changes as the flood occurred nearly a decade ago, but
133 it is clear that the images were not captured by the council but rather requested from the valley
134 residents. The 32 interpretable photos are thus treated as “crowd-sourced” observations here
135 and used for hydraulic model calibration (shown in Figure 2 alongside example photos).
136 Interpreting water levels from crowd-sourced field photos of flooding is out of scope for this
137 manuscript, however, recent advances in deep learning suggest that automatic derivation at
138 scale could be possible soon (e.g. Chaudhary et al. 2020).

139 It is worth noting that a much larger number of photographs were available to the
140 council (145), but only 32 of these turned out to be useful for the interpretation of water levels.
141 The conundrum of available vs. usable data is representative of any crowd-sourcing based data
142 collection exercise, where the available data quantity typically exceeds the amount of actually

¹ <https://www.flickr.com/photos/50615476@N03/8503268526/in/pool-abcnorthcoast/>

² https://www.facebook.com/GraftonAustraliaFloods2013/about/?ref=page_internal

³ <https://www.dailytelegraph.com.au/news/nsw/grafton/floods-maclean-tuesday-january-29-2013/image-gallery/744379f7b46246989ec0a7133346cbb9>

⁴ <https://www.dailytelegraph.com.au/news/nsw/grafton/floods-yamba-wednesday-january-30-2013/image-gallery/2e101b950af514999f487beffccb3b97?page=4>

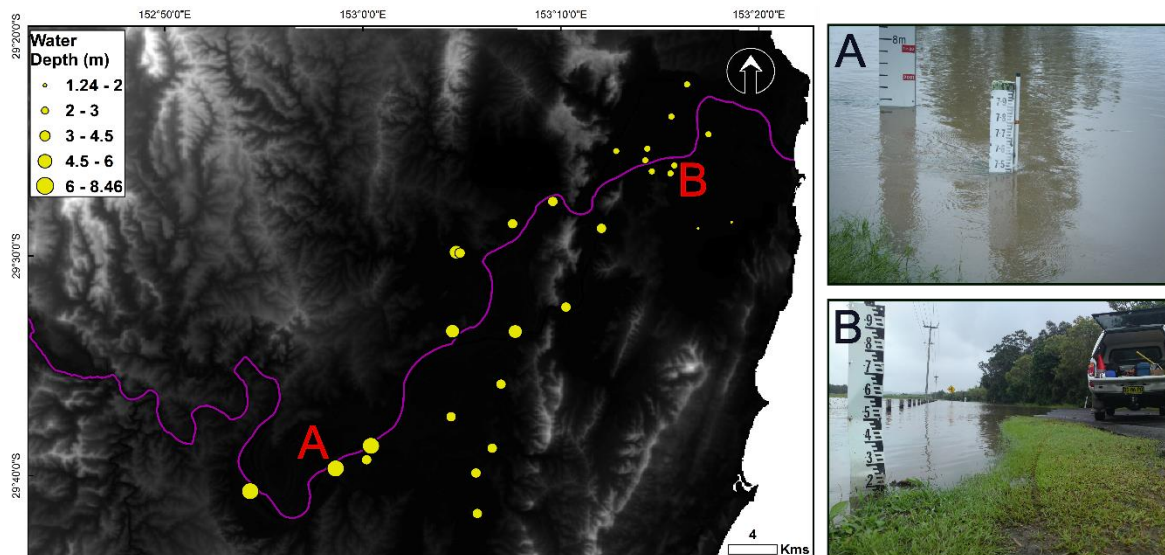


Figure 2. Locations of the “crowd-sourced” water depth observations for the 2013 flood event in the Clarence Catchment. Sub-figures A and B show example images used for the depth calculation, interpreted and provided by the Clarence Valley Council.

143 usable data. However, studies have demonstrated the value of including even a few independent
 144 crowd-sourced points (e.g. 20-50) to improve the quality of flood mapping from satellites by
 145 providing complementary information on flood inundation (see Sunkara et al. 2020 for further
 146 details). Furthermore, many of the residents of the Clarence area had recently lived through
 147 record flooding in 2011, which may have contributed to their understanding of some flood
 148 processes and in turn influenced the quality of the submitted photographs. It could be argued
 149 that these many observations or the data collection procedure, are not enough to be qualified
 150 as “crowd-sourced” data, which is typically characterized by larger data volumes. However,
 151 on considering the acquisition and collection techniques described above, the dataset is
 152 classified as crowd-sourced and not a citizen science dataset, since the engagement with the
 153 citizens only extended to requesting any/all event photos.

154 Hydrometric gauge information was provided by the NSW Public Work's Manly
 155 Hydraulics Laboratory (MHL) and the Australian Bureau of Meteorology (BoM). The

156 observations were recorded with a temporal frequency of fifteen minutes for the WL gauges.
 157 Missing data were interpolated using linear interpolation for WL observations available at
 158 Rogan’s Bridge, Grafton, Ulmarra, Brushgrove, Lawrence, Maclean, Palmer’s Island Bridge,
 159 and Yamba, from upstream to downstream along the main stem of the river. Gauge locations
 160 are shown in Figure 1, while hydrographs recorded by gauges along the main stem of the
 161 channel are shown in Figure 3 for the 2013 flood event. Additionally, WL observations were
 162 available at Tyndale, The Avenue, Oyster Channel, and Lake Wooloweyah. The WL values
 163 were recorded in meters with respect to AHD and used to verify the channel friction parameter
 164 identified using crowd-sourced observations.

165 Topographic information was available in the form of a 1 m Light Detection And
 166 Ranging (LiDAR) bare earth Digital Elevation Model (DEM), acquired between 2001 and 2015

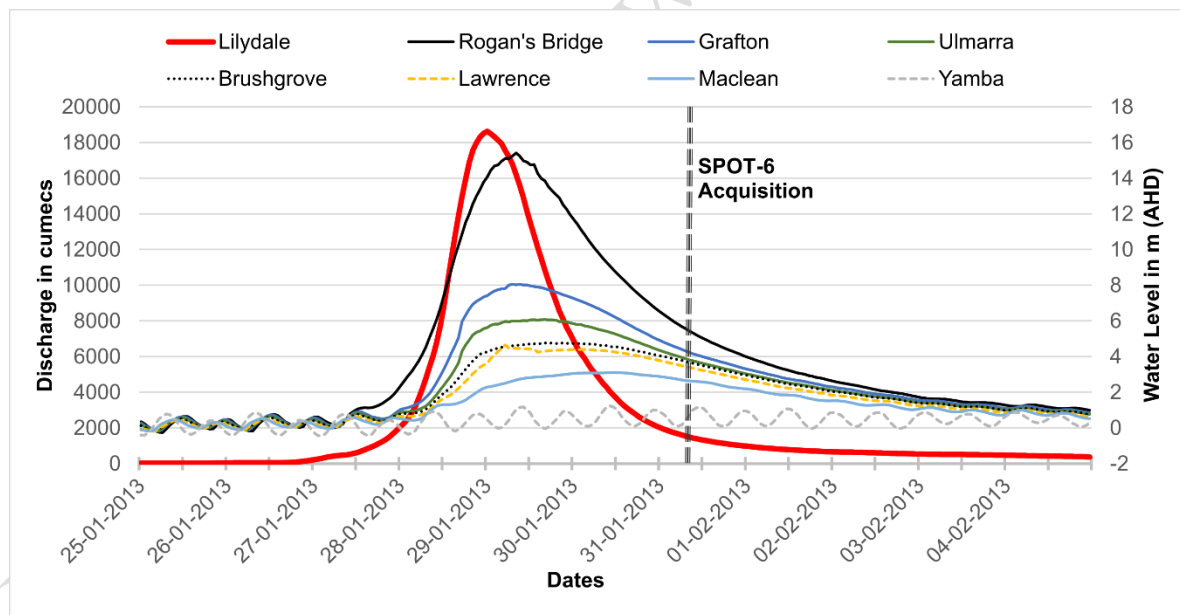


Figure 3. Hydrographs recorded at the hydrometric gauges along the main stem of the Clarence River (locations shown in Figure 1) for the 2013 flood event, shown together with the temporal acquisition of available remote sensing data. The shaded hydrograph refers to the inflow boundary condition at Lilydale.

167 with a vertical accuracy of ± 30 cm and horizontal accuracy of ± 80 cm (New South Wales Land
168 and Property Management Authority, 2010; Figure 4). This dataset is freely available under a
169 Creative Commons Attribution 4.0 license, for commercial and non-commercial applications
170 at <https://elevation.fsd.org.au/>, provided by Geoscience Australia. The channel bathymetry
171 was reconstructed by interpolating between field-observed cross-sections and stitched to the
172 LiDAR DEM, for the part of the domain where it was available. Bathymetric data were
173 collected during a field campaign in 2015 (Grimaldi et al., 2017), described extensively in
174 Grimaldi et al. (2018), and supplemented with pre-existing bathymetric datasets (Farr &
175 Huxley 2013). The area upstream of Copmanhurst where LiDAR coverage was unavailable,
176 was in-filled with the SRTM-derived 30 m product.

177 An optical multi-spectral image from the Satellite Pour l'Observation de la Terre
178 (SPOT) 6 satellite was available to this study (Figure 4), acquired on January 31 2013 at 09:35
179 AM (AEDT). The data were acquired at 6 m resolution and delivered as an ortho-rectified, pan-
180 sharpened multi-spectral (PMS) product at 1.5 m with four spectral bands, i.e. blue (450-520
181 nm), green (530-590 nm), red (625-695 nm), and near infrared (760-890 nm). SPOT-6 PMS
182 products have a radiometric resolution of 12 bits per pixel and the image was delivered in the
183 JPEG 2000 raster format (Astrium Services 2013). The image comprised of a total of 250
184 million pixels covering a total area of 573.91 km². About 25% of the tile was affected by cloud
185 cover, obscuring the underlying inundated regions. In order to avoid the associated uncertainty,
186 this portion of the image was removed from the analysis.

187 Figure 4 shows the spatial extent of the SPOT image with respect to the model domain,
188 along with the temporal position with respect to the 2013 flood hydrographs. This image was
189 converted to Normalized Differential Water Index (NDWI) (McFeeters 1996) values to
190 delineate the flood waters. The true colour composite of the SPOT image is juxtaposed against
191 the derived NDWI image in Figure 6. Problems of flood monitoring using optical data are

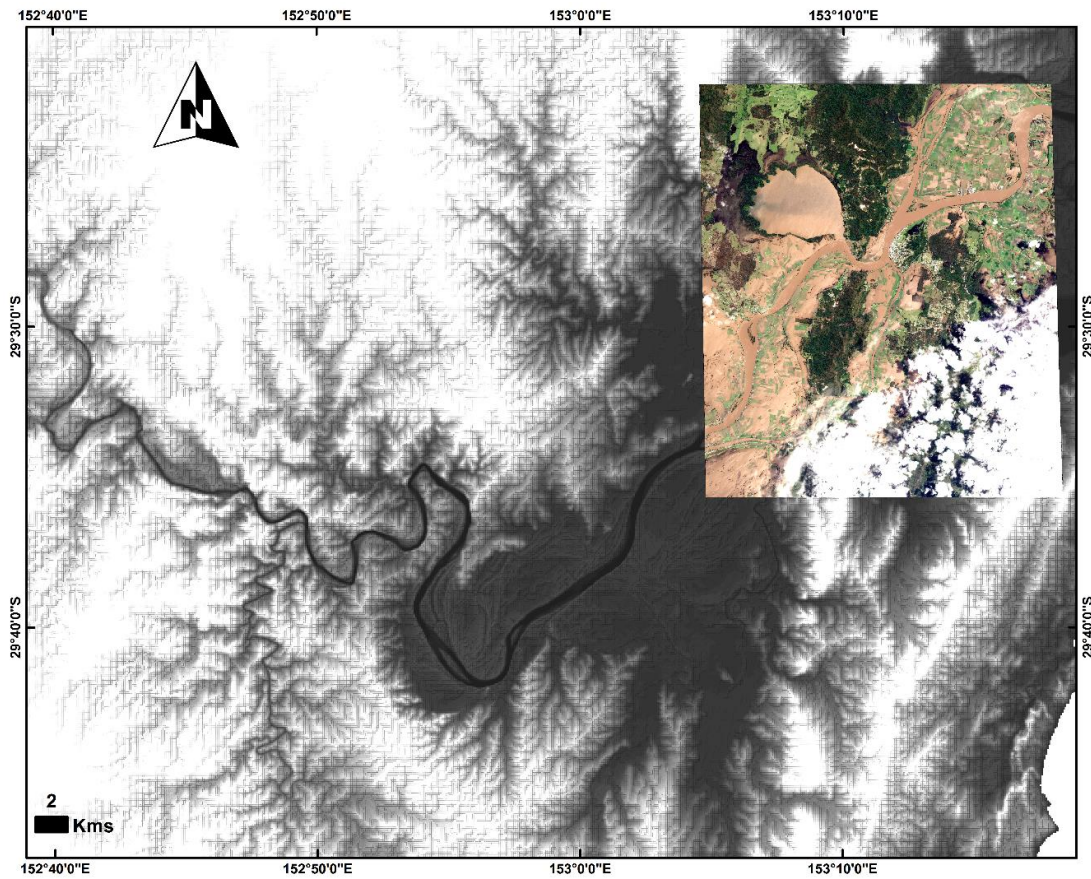


Figure 4. Spatial extent of the SPOT-6 optical image covering the 2013 flood event in the Clarence, shown here with respect to the model domain. The LiDAR DEM available to this study is used as the base layer.

192 apparent, as nearly 25% of the image is unusable due to cloud cover. Although the initial
 193 formula for the calculation of NDWI was developed for applications to the Landsat Multi
 194 Spectral Scanner (MSS) sensors, it has since been extended to all optical satellites (McFeeters
 195 2013). The general equation used for calculation of NDWI in this study is given as

$$196 \quad NDWI = \frac{Green - NIR}{Green + NIR}, \quad (1)$$

197 where NIR refers to the Near-Infrared channel.

198 **4 Methods**

199 The overall methodology for this component of the research is summarized in Figure
200 5.

201 **4.1 Model Implementation**

202 The LISFLOOD-FP inertial acceleration solver was implemented in full 2D for the
203 Clarence Catchment at 30 m grid resolution, as Grimaldi et al. (2018) found it a cost-effective
204 modelling solution for the Clarence Catchment. Implementation of this model requires a DEM,
205 river geometry information, boundary conditions, and channel/floodplain roughness values

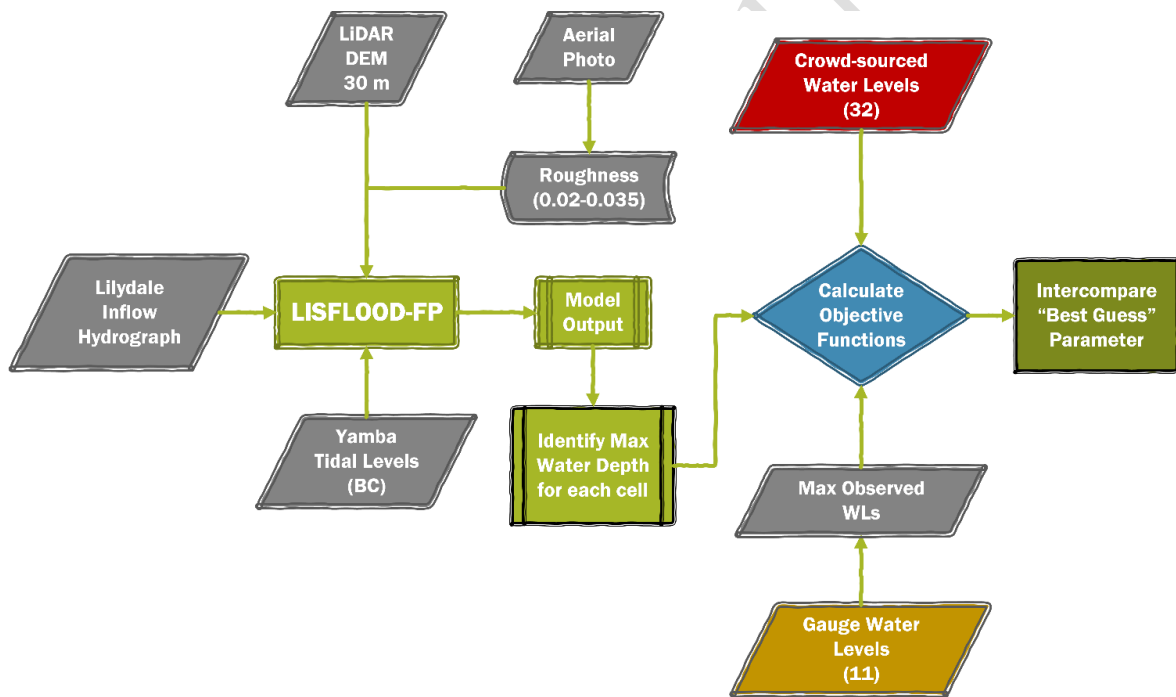


Figure 5. Schematic of overall methodology used in this paper for the parameterization of channel roughness in LISFLOOD-FP. The number of “crowd-sourced” and gauged water level locations has been included in the illustration, along with the range of roughness values considered for calibration which were identified from aerial field photographs. BC=Boundary Conditions; WLS=Water Levels.

206 which can be specified as lumped or distributed. For the floodplain, spatially distributed
207 roughness values were assigned based on Arcement & Schneider (1989) recommendations for
208 given land-uses, which in turn were assessed using field and aerial photographs. This spatially
209 distributed floodplain roughness map was used consistently throughout this study, for all the
210 “lumped” channel roughness calibration experiments. The only exception from this are the
211 floodplain roughness tests described in Section 4.2. The discharge measurements available at
212 the Lilydale gauging station were used as the upstream boundary (Neumann condition). Tidal
213 water levels observed at Yamba were similarly used as the downstream boundary condition
214 (Dirichlet condition), see Figure 1 for the locations of Lilydale and Yamba, which form the
215 boundaries of the study reach. Lateral inflows were not included in the model setup, as they
216 did not contribute significant water volumes during the 2013 flood event, which was dominated
217 by a combination of high rainfall and tidal levels (Rogencamp 2004).

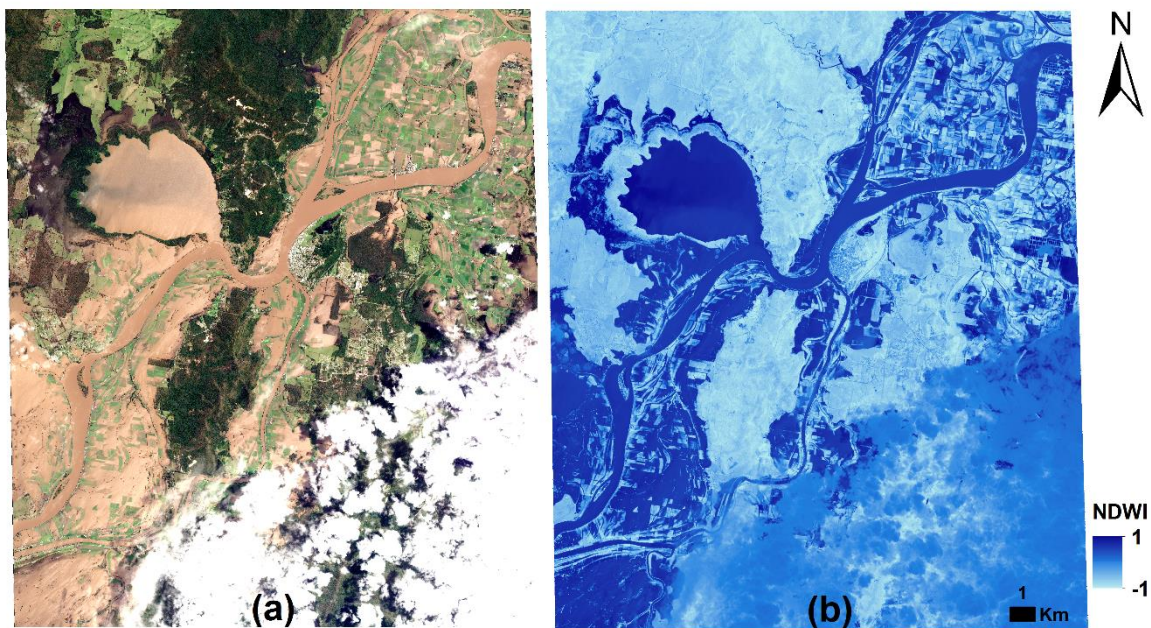


Figure 6. Optical multispectral imagery from the SPOT-6 satellite, with (a) showing a true colour composite of the area, and (b) showing the Normalized Differential Water Index values derived from (a).

218 Using tidal water levels as the downstream boundary, additionally allowed the
219 evaluation of backwater effects on floodplain inundation for this catchment. Most hydraulic
220 modelling studies choose to disaggregate spatially distributed coefficients of channel and
221 floodplain roughness, into just one spatiotemporally invariant value for each (Werner et al.
222 2005). These are generally considered as effective parameters in hydraulic modelling, used to
223 compensate for inadequate process and topographic representation (Horritt & Bates 2001; Jung
224 et al. 2012). The floodplain roughness parameter is expected to be sensitive only during high
225 velocity out-of-bank flows, as water shear will dominate resistance to flow once the floodplain
226 is already wet (Mason et al. 2003; Schumann et al. 2007). As the events analysed in this paper
227 were between 20 and 30 year return period floods, distributed time invariant values of
228 floodplain roughness were assigned based on the land-use and kept constant for all runs.

229 **4.2 Model Calibration**

230 Channel roughness is the only calibration parameter for this particular model
231 implementation, which primarily controls the flood wave arrival time. Here, a lumped
232 Manning's n value for the channel was optimized from 0.020 to 0.035 $\text{s/m}^{1/3}$, which is the
233 seasonal range of values for the Clarence River, by varying it in increments of 0.001 $\text{s/m}^{1/3}$
234 (Farr & Huxley 2013). This range was selected based on preliminary tests whereby a well-
235 performing range was selected for further refinement of the model. Starting with 32 uniformly
236 spaced Manning's n values, within the range of possible values for the channel friction (0.01
237 to 0.1 $\text{s/m}^{1/3}$), the hydraulic model was run using a distributed land-use based floodplain
238 roughness map. The channel roughness range was selected according to the Kling-Gupta
239 Efficiency (KGE; Gupta et al. 2009) as calculated for a few select gauges and the Mean
240 Absolute Bias (MAB) and Root-mean-squared-errors (RMSE) for the CS data points. In each
241 iteration 32 uniformly spaced values within the range were evaluated, and the best performing
242 range of roughness values selected for the next iteration with finer increments. Figure 7 shows

243 the plots from the parameter range refinement exercise, with subplots (a), (b), and (c), showing
244 the outcomes from the three iterations for channel roughness, and (d) for the floodplain
245 roughness. The left-axis shows the KGE values and the right axis shows the RMSE, while the
246 different coloured lines show the objective function values.

247 As these were “crowd-sourced” observations of high water marks, it is reasonable to
248 assume that they coincided with the peak flow recorded at the nearest river gauging station. In
249 the absence of adequate information on the data acquisition procedures, this assumption was
250 based on multiple previous studies where HWMs were assumed to correspond to the simulated
251 maximum water levels (see for example Di Baldassarre et al. 2009; Prestininzi et al. 2011). For
252 each model grid cell where a corresponding crowd-sourced observation was available, the
253 simulated maximum water depth (MWD) was first evaluated. Subsequently, the two chosen
254 objective functions, the Root Mean Squared Error ($RMSE_{MWD}$) and Mean Percentage
255 Difference (MPD_{MWD}) were calculated. The metrics were calculated by comparing the
256 simulated maximum water depth (Sim_{MWD}) for each model grid cell coinciding with a crowd-
257 sourced or gauge observation (i), against the crowd-sourced/gauged value (Obs_{MWD}), and then
258 averaging across all observations (m). The RMSE was chosen to quantify absolute error in the
259 simulation, while the MPD function allowed a relative error assessment with respect to the
260 observation values. The objective functions were computed as

261

$$RMSE_{MWD} = \sqrt{\frac{\sum_{i=1}^m (Sim_{MWD} - Obs_{MWD})^2}{m}}, \quad (2)$$

262
$$MPD_{MWD} = \frac{Abs(Sim_{MWD} - Obs_{MWD})}{Obs_{MWD}} \times 100, \quad (3)$$

263
$$MinE_{opt} = \min_j (RMSE_j^{MWD} \times |MPD_j^{MWD}|), \quad (4)$$

264 Here j refers to a specific roughness value and J refers to the complete set of roughness
265 values evaluated herein, over which the minima is calculated. The roughness value
266 corresponding to the minima of the product ($MinE_{opt}$) of $RMSE_{MWD}$ and MPD_{MWD} , was
267 selected as the best performing parameter n_{opt} from all the tested roughness values. The
268 product was considered as it is a simplified approach towards multi-objective optimization, as
269 both objective functions needed to be minimized. Furthermore, the product was chosen over
270 the sum as it further inflates the objective function values, amplifying the variability captured
271 by the metric and helping to differentiate between models with only slight differences in
272 performance. As the information content of the observations is distributed in space but limited
273 in time, it is postulated that using more than one objective function with different priorities will
274 allow for a more robust evaluation (Zhang et al. 2013). Best fit parameters identified by using
275 crowd-sourced and gauged water levels (using only the flood peak value, since it was the only
276 information consistently available across all data sources), were inter-compared to assess the
277 information content of the crowd-sourced data. The maximum water depth values computed
278 by the numerical model were finally compared with crowd-sourced and gauged water levels to
279 arrive at the calibrated parameter value.

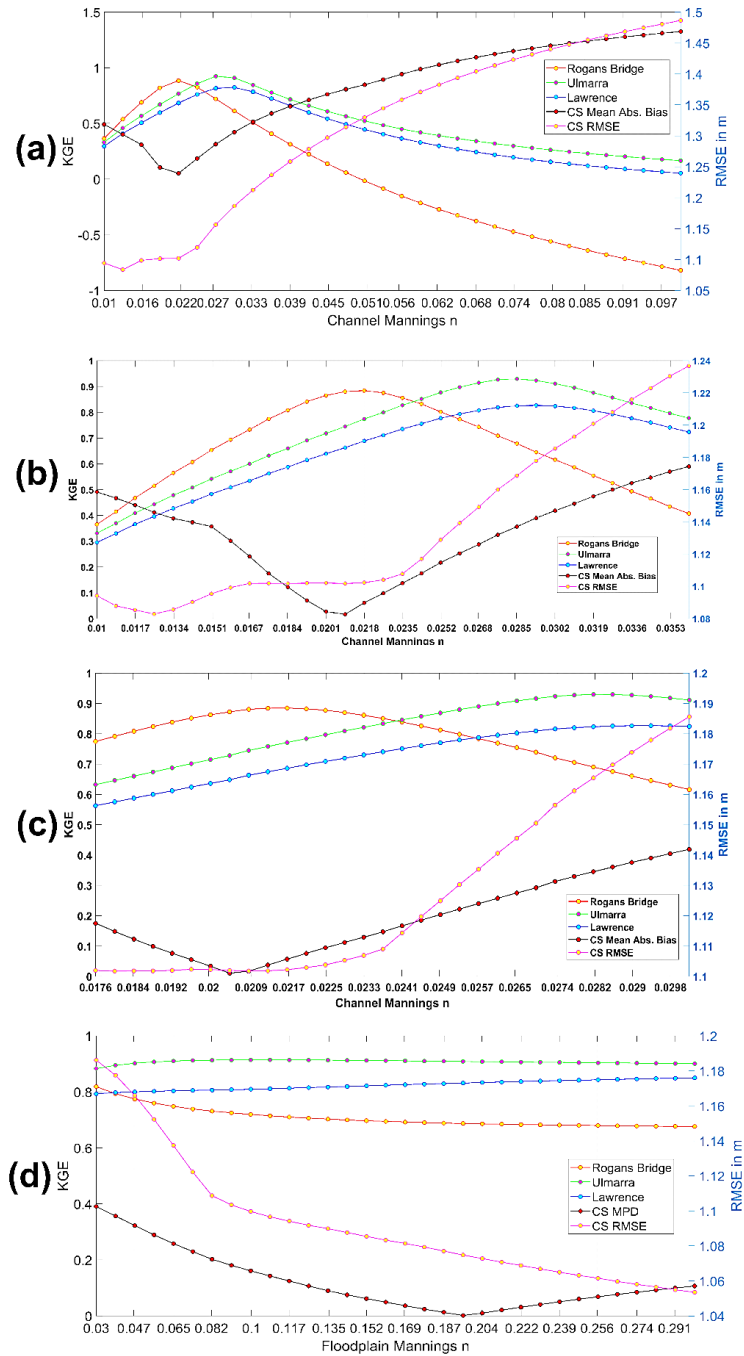


Figure 7. Plots showing the iterative parameter range refinement exercise, with (a), (b), and (c) showing the impact of changing the channel Manning's roughness on the Mean Absolute Bias (MAB) and Root Mean Squared Errors (RMSE) for all the crowd-sourced points and the Kling Gupta Efficiency (KGE) for a few selected gauges. A similar analysis for the floodplain friction is shown in (d). Note that all lines are plotted on the primary axis (KGE), even the black line for the MAB of the CS points, with the exception being the pink line for the CS observations' RMSE plotted on the secondary axis.

280 **4.3 Model Validation**

281 Parameter values chosen through the procedures outlined in the previous section were
282 additionally verified using NDWI values from an independent optical remote sensing dataset,
283 to ensure reliability of the simulated inundation patterns. NDWI uses features of the water
284 reflectance spectrum, i.e. maximum reflectance in the green region of the electromagnetic
285 spectrum and minimum in the NIR region, to enhance the identifiability of water surfaces. It
286 also exploits the high reflectance of terrestrial vegetation and soil in the NIR region to aid the
287 delineation of water bodies (McFeeters 1996). While using a band ratio approach for surface
288 water detection does not eliminate uncertainties (Mukherjee & Samuel 2016); the objective
289 here was just to achieve an acceptable model set up, which was considered sufficient to verify
290 the parameter choices (Andreadis & Schumann 2014).

291 NDWI values larger than 0 are typically expected to represent water pixels, while
292 negative values represent non-water land-use classes (Jain et al. 2005; Lu et al. 2011).
293 Accordingly, the cloud-free portion of the SPOT image was processed to derive NDWI values,
294 which was subsequently converted into a surface water map using a global threshold of 0 to
295 retain positive values. NDWI values were derived from the SPOT image at the native resolution
296 (1.5 m) of the pan-sharpened product, although these had to be upscaled to the model grid size
297 of 90 m prior to making any comparisons. Model simulated water depths were extracted at the
298 time of acquisition of the SPOT image and converted to inundation extent maps using a
299 threshold of 1 cm. This depth threshold was used to derive flood extents throughout this paper.
300 Although some studies have justified the use of a 10 cm depth threshold for reasons of
301 uncertainty (Pappenberger et al. 2007), it also means that a pixel with 9 cm water depth will
302 not be considered inundated. This implies that 729 cubic meters of model simulated water
303 volume per pixel was ignored during the flood extent assimilation process. Consequently, a
304 threshold of 1 cm was considered more suitable in this study (Hostache et al. 2018).

305 Finally, the calibrated model performance was quantified through contingency maps
 306 and confusion matrix-based performance measures. The confusion matrix is composed of four
 307 values, which in this study were defined as follows: the number of pixels correctly simulated
 308 as flooded (hits), the number of pixels simulated as flooded but dry in the observation (false
 309 alarms), the number of simulated dry but flooded in the observation (misses), and the number
 310 of pixels correctly predicted as non-flooded (correct rejects). The critical success index (*CSI*;
 311 Donaldson et al., 1975), and Cohen's kappa (Cohen, 1960) were used, as they are commonly
 312 used for binary pattern matching (Stephens et al. 2014). The performance measures were
 313 calculated as

$$314 \quad CSI = \frac{hits}{hits+misses+false\ alarms}, \quad (5)$$

$$315 \quad Kappa = \frac{2 \times (hits \times correct\ rejects - misses \times false\ alarms)}{(hits+false\ alarms) \times (false\ alarms+correct\ rejects) + (hits+misses) \times (misses+correct\ rejects)} \quad (6)$$

316 The critical success index corrects for the over-representation of the correct rejects in
 317 the model domain, while the kappa coefficient corrects for expected chance agreement. These
 318 metrics quantify goodness of fit; they attain their highest value of 1 when the predictions
 319 provide a perfect fit to the observations.

320 Due to the limitations of optical satellite imagery, which is unable to penetrate
 321 vegetation canopies and is thus incapable of detecting flood waters under vegetation.
 322 Accordingly, the Normalized Differential Vegetation Index (Wang et al. 2011), was also
 323 computed for the SPOT-6 image, to verify whether the binary mismatch between the model
 324 and the satellite observation was caused by actual disagreement or the inability of the sensor to
 325 map inundation. NDVI leverages the difference in the spectral response of the chlorophyll-
 326 loaded vegetal tissues in the red and infra-red channels of multispectral satellites, which higher
 327 values indicating high density and typical values ranging from 0.1-0.7 for vegetated areas

328 (Jarlan et al. 2008). While there is no clear consensus in literature on the lower bound of NDVI
329 values for vegetation or at which vegetation density optical sensors become unusable,
330 investigating these questions was outside the scope of this manuscript. Here the general
331 threshold of 0.1 to identify vegetation is used as a threshold, since the NDVI is only used as a
332 reference to facilitate a qualitative assessment of the model validation.

333 **5 Results and Discussion**

334 **5.1 Model Calibration**

335 This section presents the results obtained from this novel calibration exercise based on
336 crowd-sourced data and discusses the possible implications of this analysis. First, the model
337 simulations of maximum water depth for different channel roughness values were compared
338 with the crowd-sourced observations. Consequently, the maximum water level values for each
339 cell containing a water mark were compared with the maximum value within the corresponding
340 grid cell for the flood inundation model simulation. In other words, the timing of the maximum
341 water level was not considered, which may impact the accurate simulation of the flood wave
342 arrival and travel times. Since water level values represent the sum of the flood water depth
343 and the underlying DEM, the vertical uncertainty in the DEM could influence the calibration
344 outcomes. Indeed, it is possible to obtain positive/negative errors for all the simulations due to
345 DEM uncertainty. However, the impact of the DEM uncertainty was not explicitly investigated
346 in this study as the focus was on the use of crowd-sourced water levels for model calibration.

347 Figure 8 shows the distribution of the RMSE and MPD values for the considered range
348 of the channel roughness parameter, as compared to the crowd-sourced water level values. In
349 this study, spatial variability in the roughness parameter was not considered, since adequate
350 data to resolve grid-wise parameters in two-dimensional space were not available. Moreover,
351 hydraulic model uncertainties in the forecast mode are predominantly a function of topography

352 and inflows (Andreadis & Schumann 2014) as previously discussed. Consequently, the impact
 353 of spatial heterogeneity in the roughness characterization was not expected to yield notably
 354 different results (Giustarini et al. 2011).

355 The maximum RMSE across the 15 simulations within the selected “optimal” range of
 356 Manning’s values was ~0.5 m and the maximum MPD ~40%, which could be the reason for
 357 the low variability of the model performance. Hostache et al. (2009) reported ± 40 cm RMSE
 358 through traditional calibration using a downstream limnigraph, where a LiDAR DEM with ± 15
 359 cm and observed cross-sections with up to ± 30 cm uncertainty were used. The variation

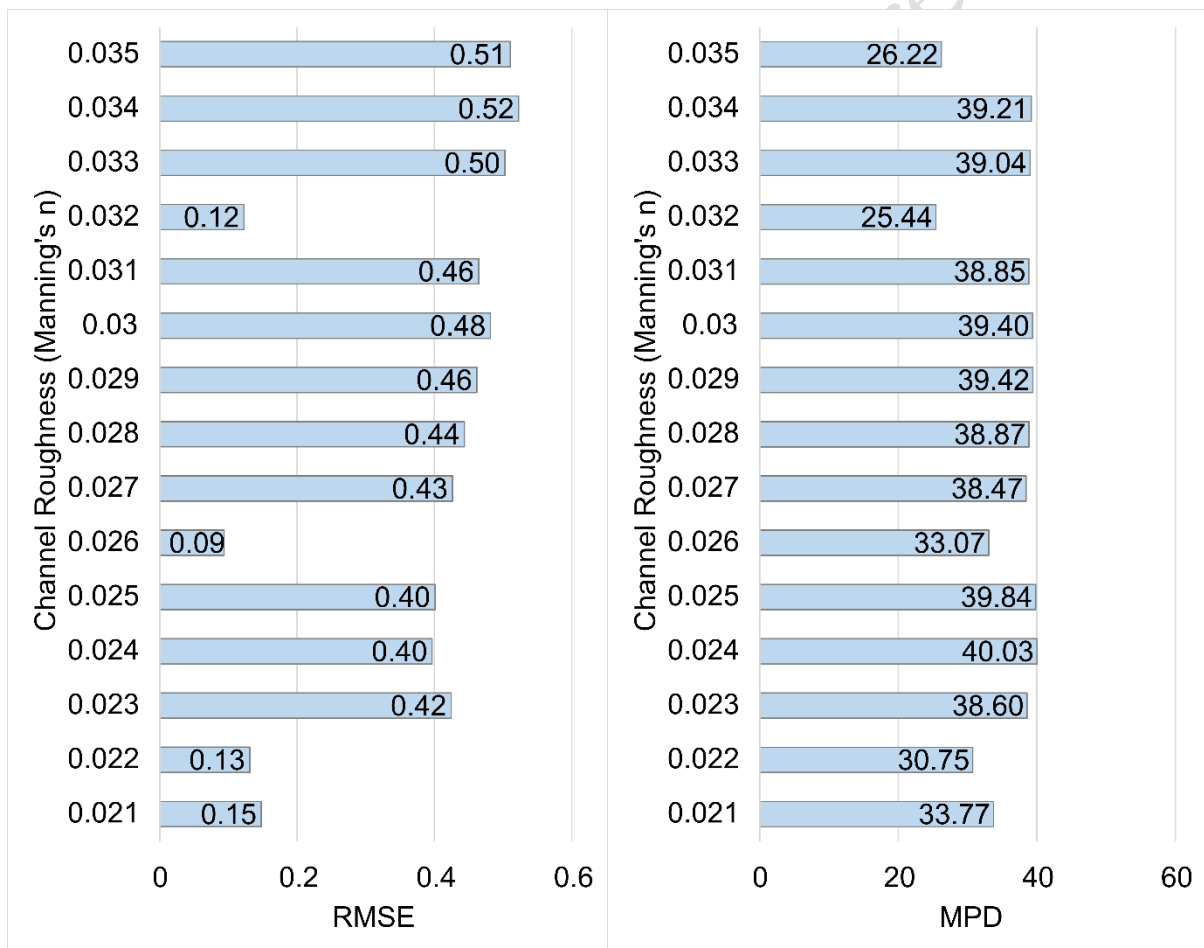


Figure 8. Maximum water levels simulated by LISFLOOD-FP compared with crowd-sourced observations, with the plot on the left showing the root mean squared error (RMSE) values and the mean percent difference (MPD) values on the right.

360 observed across the values of RMSE and MPD for the evaluated roughness range implies high
361 parameter sensitivity. As the channel roughness controls the flood wave arrival time and the
362 time of channel over-topping to some extent, which in turn influences flood plain water levels,
363 the observed sensitivity was expected despite these factors not being explicitly considered.

364 The variation in the objective function values display no particular trend. Manning's n
365 values of 0.026 and 0.032 seemed to perform well across both metrics, with RMSE values of
366 9 and 12 cm, respectively, and MPD values of 33.07% and 25.44%, respectively. Based on the
367 multi-objective performance evaluated from Figure 8, $n = 0.026$ was clearly the better choice,
368 in comparison to the crowd-sourced water level observations. This choice is driven by the low
369 absolute errors (RMSE) observed for this roughness value which compensate for the relatively
370 higher value of relative errors (MPD), due to the nature of the objective function which is
371 designed as a product.

372 The objective function values at $n = 0.026$ are substantially lower than the
373 neighbouring Manning's values tested suggesting that it could be a local anomaly. One of the
374 reasons for this could be the use of a uniform channel roughness value and the spatial
375 distribution of the crowd-sourced points being skewed towards the downstream part of the
376 catchment. Due to the uneven distribution, the calibration process will inevitably prioritize
377 those effective parameterizations, which best simulate the inundation dynamics in this region.
378 It is thus possible that those roughness values which best reproduced the channel over-topping
379 time and the superposition of the tidal and flood waves in this region would be selected using
380 the methods proposed here. This value can also be a local minima as observed from Figure 8,
381 as the crowd-sourced points are only able to provide information on the floodplain in the lower
382 part of the catchment (Pappenberger et al. 2005). Moreover, the distribution of the points is
383 sometimes really close to the channel, e.g. the points at Grafton or sometimes really far out
384 into the floodplain, which would mean that an effective roughness value that performs equally

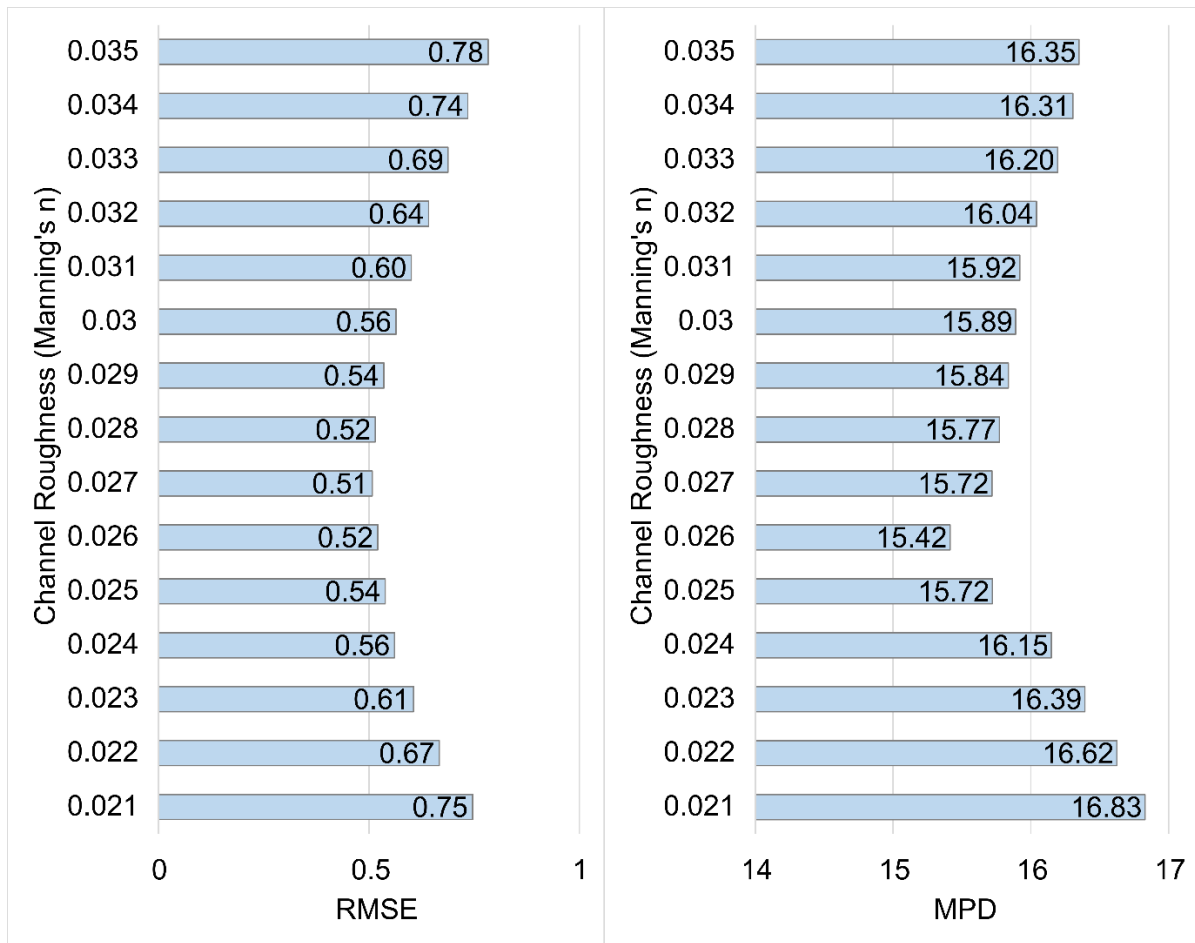


Figure 9. As for Figure 8 but for the maximum water levels simulated/observed at gauge locations.

385 well at both locations must be identified (Mukolwe et al. 2016). Perhaps this is not the case for
 386 the neighbouring values thus resulting in notably lower RMSE values for $n = 0.026$. Due to
 387 the nature of the hydraulic model uncertainties and the equifinality of model parameters, it is
 388 possible that a local minima best compensates for localized bathymetric errors, for instance
 389 (Beven 2006).

390 In contrast to the previous comparison with crowd-sourced water levels, there is a clear
 391 trend in the objective function values when inter-comparing the simulated maximum water
 392 level values with the gauged observations shown in Figure 9. Here, the modelled and measured
 393 maximum water levels at the gauge locations were inter-compared regardless of the

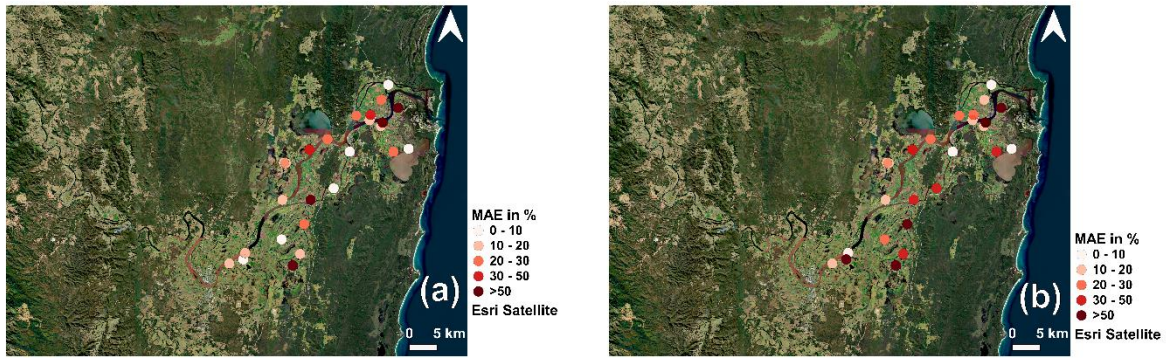


Figure 10. Maps of the model domain showing the spatial distribution of the crowd-sourced points and the corresponding mean absolute error percentages for simulated water levels produced by using a channel friction value in Manning's n of (a) $n=0.026$ and (b) $n=0.032$.

394 information on the timing of the flood peak. The values of both error metrics first increased
 395 with a corresponding increase in the magnitude of the channel roughness, then decreased after
 396 the optima. The maximum RMSE across all simulations was ~ 78 cm and the maximum MPD
 397 $\sim 17\%$, again indicating a suitable model setup. These findings are aligned well with the
 398 expectations; as the water depth in the channel is larger, the corresponding RMSE or the
 399 absolute error is higher. Low values of the MPD imply that the percentage error was actually
 400 lower than what was observed in the previous test against crowd-sourced water levels in the
 401 floodplain. Moreover, the variability in both absolute and relative errors was lower than in the
 402 case of crowd-sourced water levels. Again, this was expected as the water level variation within
 403 the confines of the channel might not be as much as is possible in the floodplains.

404 In this experiment, Manning's n values between 0.025 and 0.028 seemed to perform
 405 well across both error metrics. Upon further examination of the two objective functions, $n =$
 406 0.026 appeared to be the clear choice again. The trend observable in Figure 9, where a nearly
 407 concave response to changes in the roughness values can be observed for both absolute and
 408 relative errors based on the objective functions, with a clearly global minima detected at $n =$

409 0.026. This finding corroborates the hypothesis that the Manning's roughness value selected
410 based on Figure 8 was a good overall fit for the channel, and the apparent "local minima" is
411 simply an artefact of the calibration prioritizing model accuracy primarily in the downstream
412 region. In order to further investigate the impact of the spatial distribution and outliers on the
413 evaluated objective functions, the MPD and bias values for the two well-performing parameter
414 choices in case of the crowd-sourced data were plotted in Figure 10 and Figure 11, respectively.

415 For the MPD maps in Figure 10, the channel roughness value of Manning's $n = 0.026$
416 shown in (a) was driven by a small number of highly erroneous points (darker shades of red)
417 towards the downstream end of the model domain and in the storages southeast of Grafton.
418 Conversely, the MPD values for channel roughness corresponding to $n = 0.032$ shown in (b),
419 exhibit larger errors in general (low number of light coloured points, with most in medium to
420 dark hues). Similar trends can be observed in the maps shown in Figure 11, showing the bias
421 in simulated water depth where the direction of the bias in the model is also evident. Generally,
422 the model over-predicts the water levels closer to the channel and under predict them further
423 in the floodplains. A channel roughness value of $n = 0.026$ in (a), mostly overestimates the
424 WLS at the first glance (lots of blue points), but a closer look reveals that a large number of
425 points are within ± 10 cm (white points), while others are still in lower error categories. In (b),
426 a friction value of $n = 0.032$ led mostly to large positive (dark blue points) or negative errors
427 (dark red points), with the number of low error points being very low. This analysis further
428 confirmed the choice of channel roughness as $n = 0.026$, as it produced a more consistently
429 accurate performance across the domain.

430 Despite the acceptable quality of the fit, the positive MPD values obtained in both
431 experiments implied that the model consistently underestimated the water levels at the gauges
432 and at the crowd-sourced observation locations in the flood plain. The magnitude of
433 underestimation increased with distance from the channel, which could in part be related to

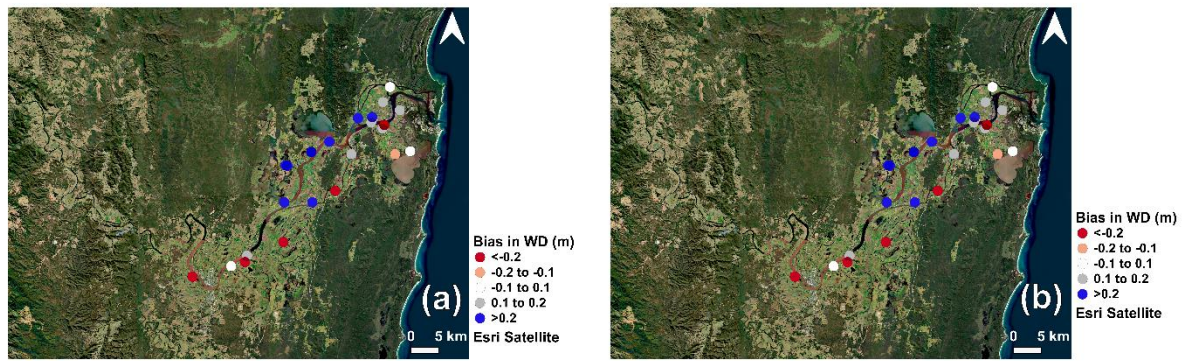


Figure 11. As for Figure 10, but for bias in water depth (m).

434 errors in the bathymetry. Only the meandering portion of the channel between Copmanhurst
 435 and Mountainview, upstream of Grafton was surveyed recently (in 2015). It thus seems
 436 plausible that the model simulations at the crowd-sourced observation locations further
 437 downstream, were strongly impacted by the poorer quality bathymetry information. Indeed, the
 438 bathymetry downstream of Grafton until Brushgrove was surveyed in the 1960s and
 439 extrapolated further downstream using a local along-thalweg curvilinear interpolation
 440 (Grimaldi et al. 2018). Moreover, the accuracy of the bathymetric survey in this area or the
 441 interpolation were unknown, and therefore cannot be used to further diagnose the model
 442 performance here.

443 Given that channel bathymetry is a highly dynamic geomorphological feature which
 444 alters with changes in the flow regime or even large flood events, it is expected that the 1960s
 445 datasets could misrepresent the channel geometry. In order to obtain a better fit to the
 446 observations, distributed friction values might be required to adequately replicate the flow
 447 patterns in the downstream portion of the catchment. However, since the fit was adequate
 448 (mean RMSE ~ 50 cm), a lumped value was considered sufficient to answer the research
 449 questions posed in this study, where the aim was to assess the utility of crowd-sourced
 450 observations for hydraulic model calibration.

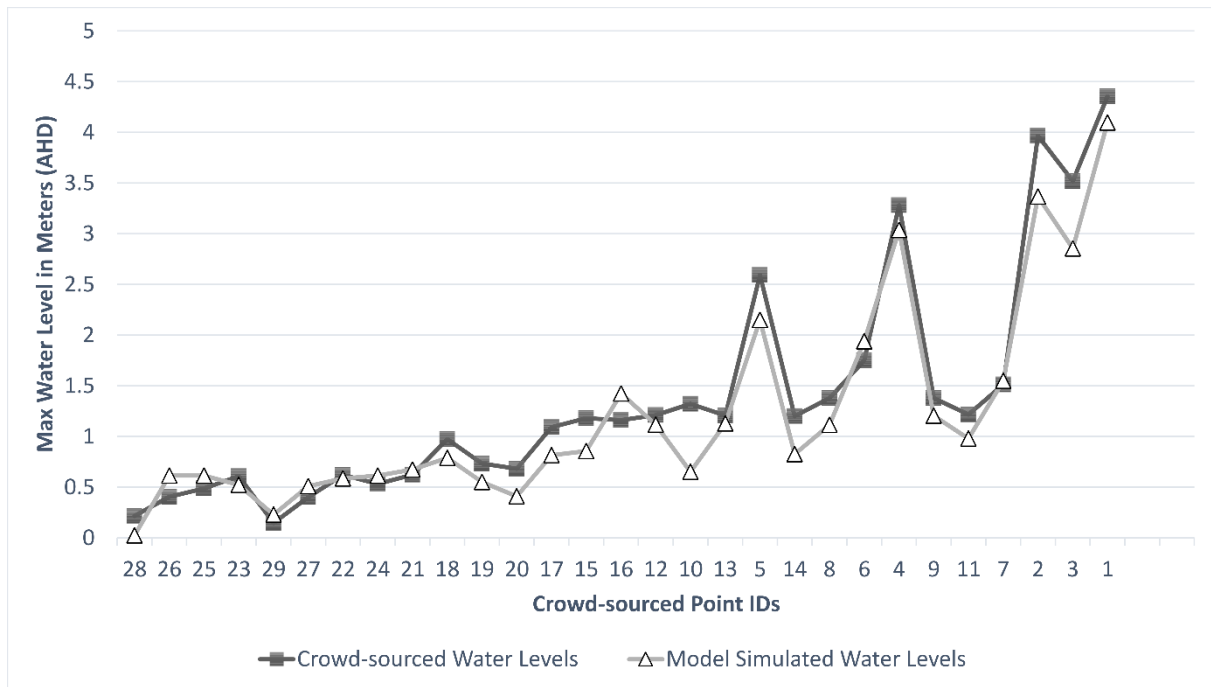


Figure 12. Plot showing the maximum water levels simulated by the calibrated model using $n = 0.026$ and the crowd-sourced maximum water levels at all the available locations. Crowd-sourced point locations have been arranged from upstream to downstream.

451 5.2 Best-fit Parameter Verification

452 From this investigation, it was concluded that the best performing value for the channel
 453 roughness parameter was $n = 0.026$, which was chosen for further verification. Figure 12 and
 454 Figure 13 show plots of the simulated and observed water depths, for crowd-sourced and
 455 gauged data points, respectively. When examined in a distributed fashion there was no clear
 456 trend in the discrepancies between modelled and observed values from upstream to
 457 downstream (gauge locations are shown in Figure 1), i.e. the model sometimes overestimated
 458 and sometimes underestimated the measurements. Due to the relatively flat geomorphology of
 459 the region, larger values of water depth were observed within the channel associated with
 460 higher error magnitudes as expected; conversely the error magnitudes were lower in the
 461 floodplain where elevation values are lower. The MPD was generally higher for the crowd-
 462 sourced points, as even low magnitude errors constitute a large percentage of the shallow

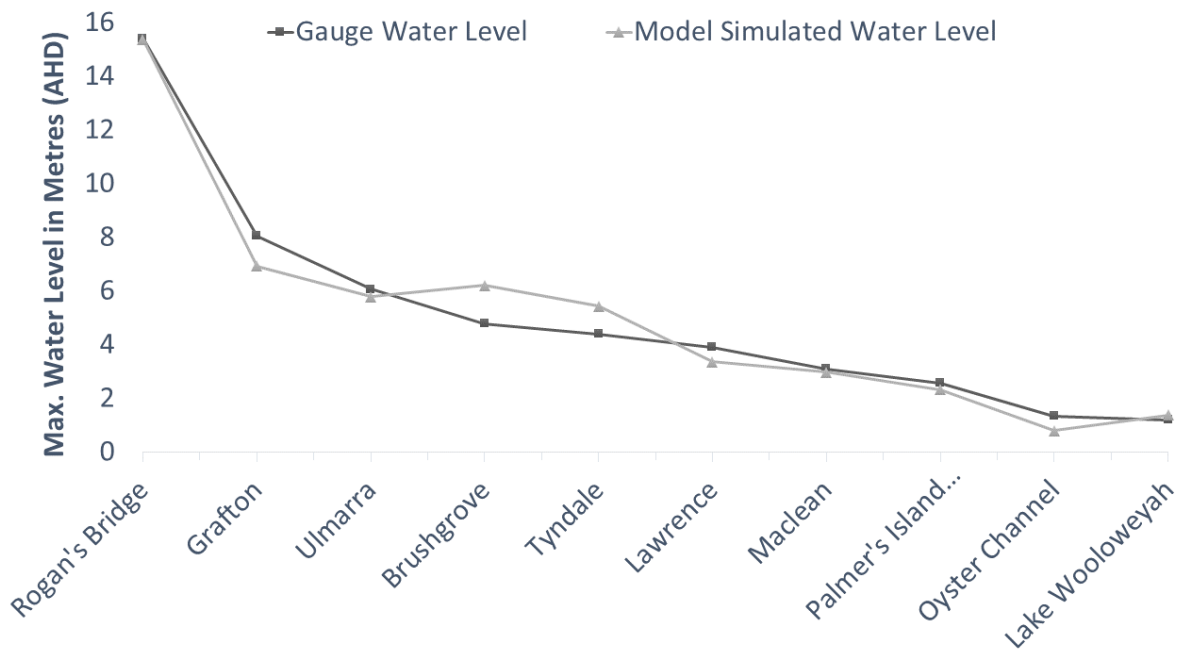


Figure 13. Plot showing the maximum water levels simulated by the calibrated model using $n = 0.026$ and the gauged maximum water depths at all the available locations. Gauges are ordered from upstream to downstream.

463 observed water depth, while the opposite was true for the gauge-based assessment within the
 464 channel.

465 Interestingly, these experiments show that in the absence of gauge information, crowd-
 466 sourced water level observations can provide sufficient information to calibrate a hydraulic
 467 model. However, this might only be true for the present case study and in the floodplains, as in
 468 the presence of a levee system, a-few-cm error in water level predictions can also cause false
 469 alarms/misses (Wing et al. 2017). In this context, there were still quite large discrepancies
 470 between gauged and modelled peak levels and perhaps the Nash-Sutcliffe efficiency (or other
 471 metrics) using the full hydrograph, would have allowed a more comprehensive evaluation of
 472 model accuracy. However, the objective of this experiment was to evaluate the potential of

473 crowd-sourced data for model calibration, assuming a severely data limited scenario which
474 may well be the case for most operational applications.

475 The number of crowd-sourced observations available to this study (32) was low
476 compared to the huge volumes of data expected from citizen science. However, these 32 high
477 water marks were highly accurate, while real crowd-sourced data might be affected by larger
478 uncertainties. As natural language processing and object extraction methods become more
479 sophisticated, the processing of text and images/videos from social media for water level
480 extraction is expected to be automated. If a large number of crowd-sourced water level
481 observations with a time stamp were made available, the present methodology could be
482 extended to accommodate those (Kutija et al. 2014), yielding further improvement in
483 parameterization accuracy. As water level extraction techniques are automated and data
484 volumes expand, model calibration may become more challenging as the inherent uncertainties
485 and errors in the data and information extraction algorithms become unavoidable. In this case,
486 the proposed methodology must be adapted to deal with this additional uncertainty, especially
487 in the absence of complementary calibration data. One approach could be to use statistical
488 techniques such as bootstrapping (e.g., Tellman et al. 2022), to cyclically select subsets of data
489 and assessing their ability to resolve the model parameters, such that highly uncertain outliers
490 can be identified and discarded. Furthermore, weighted calibration techniques may also be used
491 if the associated uncertainties are provided by the data providers or algorithm developers
492 (Pappenberger et al. 2007).

493 The primary advantage of crowd-sourcing is that calibration points can be in the
494 floodplains (Van Wesemael et al. 2019), where settlements usually exist rather than just in the
495 channel, as it should not be assumed that a hydraulic model well calibrated in the channel will
496 perform equally well in the floodplains (Pappenberger et al. 2007). Crowd-sourced water levels
497 therefore provide a unique opportunity to calibrate the model diagnostic variables in those areas

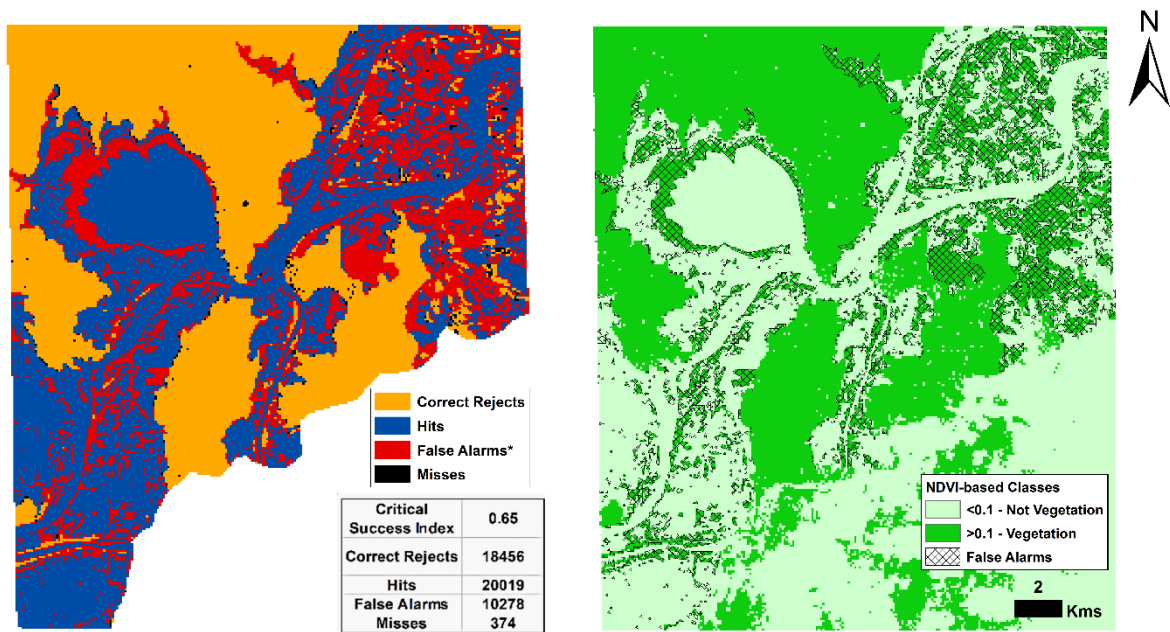


Figure 14. The left panel shows the contingency map and statistics comparing the surface water extent map based on NDWI values derived from the SPOT-6 optical image against the inundation extents simulated by the LISFLOOD-FP acceleration solver in full 2D using the calibrated channel roughness parameter. False Alarms* indicates a lack of confidence in the inundation identified through the SPOT-6 image due to dense vegetation. The right panel shows the NDVI map indicating area covered by vegetation and not vegetated regions, with respect to the extent of the False Alarms obtained.

498 where accurate estimates of flow and depth are required (Assumpção et al. 2018). In future,
 499 they may serve as complementary datasets to support remote sensing based model calibration
 500 (e.g., Tarpanelli et al. 2013; Domeneghetti et al. 2014; Wood et al. 2016; Dasgupta et al. 2020),
 501 especially to address the gaps of satellite data for such applications (see Grimaldi et al. 2016)

502 **5.3 Model Validation**

503 Interestingly, comparisons with the observed flood map yield very limited misses but a
 504 large number of false alarms. This might be related to the timing of acquisition of the SPOT-6
 505 image (Figure 3). As the image is acquired towards the end of the hydrograph, the valley is

506 already full and maximum inundation has been achieved. In such a scenario, the hydraulic flood
507 inundation models should rarely miss many flooded pixels. If rising limb images were acquired,
508 when flows are transitioning between the channel and the floodplains, the number of misses
509 and false alarms might be more comparable in the contingency maps.

510 The inset table in the left panel of Figure 14 shows a summary of the pixel statistics.
511 The number of correctly identified inundated pixels is substantially larger than the misses and
512 false alarms as noted before. It is expected that the ratio of false alarms is unrealistically high,
513 due to the misclassification of flooding under vegetation in the optical image, which is able to
514 observe only tree canopies. In order to corroborate this hypothesis, the NDVI was calculated
515 to facilitate a qualitative comparison. The right panel of Figure 14 shows the area identified as
516 “False Alarms” drawn on a base layer of the SPOT-6 NDVI-based vegetation classes. As
517 expected, most of the false alarms were perhaps flooded vegetation pixels not classified as
518 water due to limitations of NDWI-based surface water extraction from optical images.

519 In spite of the limitations outlined earlier, a Critical Success Index (CSI) value of 0.65
520 was obtained, which is in the acceptable range for flood modelling and mapping exercises
521 (Wood et al. 2016; Landuyt et al. 2018). The CSI score was found to be slightly biased towards
522 overprediction, catchment size, and event magnitude (Wealands et al. 2005; Stephens et al.
523 2014; Stephens & Bates 2015). However, as the aim was to verify the model calibration in the
524 Clarence Catchment for a single event, it was used here due to its ubiquity in flood science
525 literature. The model parameterization was therefore considered to be adequate based on this
526 analysis.

527 **6 Conclusions and Outlook**

528 This study presents the first attempt towards the use of crowd-sourced water levels for a
529 quantitative calibration of a 2D-hydraulic flood inundation model. The channel roughness

530 parameter for the hydraulic model Lisflood-FP was calibrated using a collection of 32
531 distributed floodplain water levels, derived from crowd-sourced field photographs of high
532 water marks whose timing of acquisition was unknown. Assuming that these were
533 representative of the maximum water depth observed at each pixel, quantitative performance
534 measures were used to estimate absolute and relative model errors. As a first step of model
535 verification, the calibrated parameter value was inter-compared with similar information
536 derived from hydrometric gauges, which revealed that crowd-sourcing could be a viable data
537 collection option. Furthermore, plots of maximum water depth simulated by the calibrated
538 model were compared against those obtained through crowd-sourcing and gauges, revealing
539 only minimal deviations from the observations. Finally, the inundation extent simulated by the
540 calibrated model was evaluated against an optical remote sensing image, demonstrating
541 acceptable agreement with the reliable surface water estimates extractable from the RS data.

542 This study showed that it is possible to use a limited number of accurate crowd-sourced
543 water levels to constrain a 2D-hydraulic model, especially in ungauged or flashy catchments
544 where remote sensing data is limited. The methods developed in this paper can easily be
545 extended to large volumes of crowd-sourced data, albeit the availability of an associated time
546 stamp and geolocation is necessary. In case of slight uncertainties in the timing, approaches
547 suggested by Hostache et al. (2009) could be used, where the model is forced to lie within
548 observation error limits rather than replicate the measurements. In the presence of geolocation
549 errors, the approach of Schumann et al. (2008) should be used to shift the pixel randomly in all
550 directions within the limits of the horizontal accuracy, to derive a range of possible uncertain
551 values which can then be utilised together with the aforementioned technique.

552 Many research questions still remain, such as how to objectively account for larger
553 uncertainties or how to automatically derive water levels from crowd-sourced images
554 accounting for all uncertainties. However, through this study a simple framework was

555 developed and tested, being capable of ingesting crowd-sourced water levels after a preliminary
556 quality check (Fohringer et al. 2015), successfully demonstrating their utility for flood model
557 performance assessment.

558 **Acknowledgements**

559 This study was conducted within the framework of the project “Improving flood forecast skill
560 using remote sensing data,” funded by the Bushfire and Natural Hazards CRC of Australia.
561 Additionally, gratitude is extended to the Australian Bureau of Meteorology
562 (<http://www.bom.gov.au/waterdata/>) and New South Wales Manly Hydraulics Laboratory
563 (<http://new.mhl.nsw.gov.au/>) for the gauge data, in addition to Geoscience Australia and the
564 Clarence Valley Council for sharing field and ancillary data. Antara Dasgupta was funded by
565 a PhD scholarship from the IITB-Monash Research Academy and a Postdoctoral Scholarship
566 from the University of Osnabrück.

567 **References**

- 568 Andreadis KM, Schumann GJP. 2014. Estimating the impact of satellite observations on the
569 predictability of large-scale hydraulic models. *Adv Water Resour* [Internet]. [accessed 2014
570 Aug 11] 73:44–54. <http://linkinghub.elsevier.com/retrieve/pii/S0309170814001158>
- 571 Annis A, Nardi F. 2019. Integrating VGI and 2D hydraulic models into a data assimilation
572 framework for real time flood forecasting and mapping. *Geo-Spatial Inf Sci* [Internet].
573 22(4):223–236. <https://doi.org/10.1080/10095020.2019.1626135>
- 574 Arcement GJ, Schneider VR. 1989. Guide for Selecting Manning ’ s Roughness Coefficients
575 for Natural Channels and Flood Plains United States Geological Survey Water-supply Paper
576 2339 [Internet]. [place unknown]. <http://www.fhwa.dot.gov/BRIDGE/wsp2339.pdf>
- 577 Assumpção TH, Popescu I, Jonoski A, Solomatine DP. 2018. Citizen observations

578 contributing to flood modelling : opportunities and challenges. Hydrol Earth Syst Sci.
579 22:1473–1489.

580 Astrium Services. 2013. SPOT 6 & SPOT 7 imagery user guide. Astrium Serv.(July):vi +
581 77pp.

582 Di Baldassarre G, Schumann G, Bates P. 2009. Near real time satellite imagery to support
583 and verify timely flood modelling. Hydrol Process [Internet]. 23(5):799–803.
584 <http://jamsb.austms.org.au/courses/CSC2408/semester3/resources/ldp/abs-guide.pdf>

585 Beven K. 2006. A manifesto for the equifinality thesis. J Hydrol. 320(1–2):18–36.

586 Le Boursicaud R, Pénard L, Hauet A, Thollet F, Le Coz J. 2016. Gauging extreme floods on
587 YouTube: Application of LSPIV to home movies for the post-event determination of stream
588 discharges. Hydrol Process. 30(1):90–105.

589 Chaudhary P, D’Aronco S, Leitão JP, Schindler K, Wegner JD. 2020. Water level prediction
590 from social media images with a multi-task ranking approach. ISPRS J Photogramm Remote
591 Sens [Internet]. 167(July):252–262. <https://doi.org/10.1016/j.isprsjprs.2020.07.003>

592 Chaudhary P, D’Aronco S, Moy De Vitry M, Leitão JP, Wegner JD. 2019. Flood-Water
593 Level Estimation From Social Media Images. ISPRS Ann Photogramm Remote Sens Spat Inf
594 Sci. 4(2/W5):5–12.

595 Le Coz J, Patalano A, Collins D, Guillén NF, García CM, Smart GM, Bind J, Chiaverini A,
596 Le Boursicaud R, Dramais G, Braud I. 2016. Crowdsourced data for flood hydrology:
597 Feedback from recent citizen science projects in Argentina, France and New Zealand. J
598 Hydrol [Internet]. 541:766–777. <http://dx.doi.org/10.1016/j.jhydrol.2016.07.036>

599 Dasgupta A, Thakur PK, Gupta PK. 2020. Potential of SAR-Derived Flood Maps for
600 Hydrodynamic Model Calibration in Data Scarce Regions. J Hydrol Eng [Internet].

601 25(9):05020028. <http://ascelibrary.org/doi/10.1061/%28ASCE%29HE.1943-5584.0001988>

602 Domeneghetti A, Tarpanelli A, Brocca L, Barbetta S, Moramarco T, Castellarin A, Brath A.
603 2014. The use of remote sensing-derived water surface data for hydraulic model calibration.
604 *Remote Sens Environ* [Internet]. [accessed 2014 May 27] 149:130–141.
605 <http://linkinghub.elsevier.com/retrieve/pii/S003442571400145X>

606 Farr A, Huxley C. 2013. Lower Clarence Flood Model Update 2013. [place unknown].

607 Fohringer J, Dransch D, Kreibich H, Schroter K. 2015. Social media as an information source
608 for rapid flood inundation mapping. *Nat Hazards Earth Syst Sci*. 15(12):2725–2738.

609 Fohringer J, Dransch D, Kreibich H, Schröter K. 2015. Social media as an information source
610 for rapid flood inundation mapping. *Nat Hazards Earth Syst Sci*. 15(12):2725–2738.

611 Giustarini L, Matgen P, Hostache R, Montanari M, Plaza D, Pauwels VRN, De Lannoy GJM,
612 De Keyser R, Pfister L, Hoffmann L, Savenije HHG. 2011. Assimilating SAR-derived water
613 level data into a hydraulic model: a case study. *Hydrol Earth Syst Sci* [Internet]. [accessed
614 2014 May 31] 15(7):2349–2365. <http://www.hydrol-earth-syst-sci.net/15/2349/2011/>

615 Grimaldi S, Li Y, Pauwels VRN, Walker JP. 2016. Remote Sensing-Derived Water Extent
616 and Level to Constrain Hydraulic Flood Forecasting Models: Opportunities and Challenges.
617 *Surv Geophys* [Internet]. 37(5):977–1034. [http://link.springer.com/10.1007/s10712-016-](http://link.springer.com/10.1007/s10712-016-9378-y)
618 [9378-y](http://link.springer.com/10.1007/s10712-016-9378-y)

619 Grimaldi S, Li Y, Walker JP, Pauwels VRN. 2018. Effective Representation of River
620 Geometry in Hydraulic Flood Forecast Models. *Water Resour Res* [Internet].
621 <http://doi.wiley.com/10.1002/2017WR021765>

622 Gupta H V, Kling H, Yilmaz KK, Martinez GF. 2009. Decomposition of the mean squared
623 error and NSE performance criteria: Implications for improving hydrological modelling. *J*

624 Hydrol [Internet]. 377(1–2):80–91. <http://dx.doi.org/10.1016/j.jhydrol.2009.08.003>

625 Horritt MS, Bates PD. 2001. Effects of spatial resolution on a raster based model of flood
626 flow. *J Hydrol.* 253.

627 Hostache R, Chini M, Giustarini L, Neal J, Kavetski D, Wood M, Corato G, Pelich R,
628 Matgen P. 2018. Near-Real-Time Assimilation of SAR-Derived Flood Maps for Improving
629 Flood Forecasts. *Water Resour Res* [Internet]. 54(8):5516–5535.
630 <https://onlinelibrary.wiley.com/doi/abs/10.1029/2017WR022205>

631 Hostache R, Matgen P, Schumann G, Puech C, Hoffmann L, Pfister L. 2009. Water Level
632 Estimation and Reduction of Hydraulic Model Calibration Uncertainties Using Satellite SAR
633 Images of Floods. *IEEE Trans Geosci Remote Sens* [Internet]. 47(2):431–441.
634 <http://ieeexplore.ieee.org/document/4773470/>

635 Huxley C, Beaman F. 2014. Additional crossing of the Clarence River at Grafton: flood
636 impact, levee upgrade, and structural considerations. In: *Hydraul Struct Soc - Eng challenges*
637 *Extrem* [Internet]. Brisbane, Australia; p. 1–8.
638 <http://espace.library.uq.edu.au/view/UQ:329700>

639 Jain SK, Singh RD, Jain MK, Lohani a. K. 2005. Delineation of flood-prone areas using
640 remote sensing techniques. *Water Resour Manag.* 19(4):333–347.

641 Jarlan L, Mangiarotti S, Mougin E, Mazzega P, Hiernaux P, Le Dantec V. 2008. Assimilation
642 of SPOT/VEGETATION NDVI data into a sahelian vegetation dynamics model. *Remote*
643 *Sens Environ.* 112(4):1381–1394.

644 Jung HC, Jasinski M, Kim J-W, Shum CK, Bates P, Neal J, Lee H, Alsdorf D. 2012.
645 Calibration of two-dimensional floodplain modeling in the central Atchafalaya Basin
646 Floodway System using SAR interferometry. *Water Resour Res* [Internet]. [accessed 2014

647 May 28] 48(7):n/a-n/a. <http://doi.wiley.com/10.1029/2012WR011951>

648 Kutija V, Bertsch R, Glenis V, Alderson D, Parkin G, Walsh CL, Robinson J, Kilsby C.
649 2014. Model Validation Using Crowd-Sourced Data From a Large Pluvial Flood. 11th Int
650 Conf Hydroinformatics.:9.

651 Landuyt L, Van Wesemael A, Schumann GJ-P, Hostache R, Verhoest NEC, Van Coillie
652 FMB. 2018. Flood Mapping Based on Synthetic Aperture Radar: An Assessment of
653 Established Approaches. IEEE Trans Geosci Remote Sens [Internet]. PP:1–18.
654 <https://ieeexplore.ieee.org/document/8432448/>

655 Lopez T, Al Bitar A, Biancamaria S, Güntner A, Jäggi A. 2020. On the Use of Satellite
656 Remote Sensing to Detect Floods and Droughts at Large Scales. Surv Geophys [Internet].
657 41(6):1461–1487. <https://doi.org/10.1007/s10712-020-09618-0>

658 Lu S, Wu B, Yan N, Wang H. 2011. Water body mapping method with HJ-1A/B satellite
659 imagery. Int J Appl Earth Obs Geoinf [Internet]. 13(3):428–434.
660 <http://dx.doi.org/10.1016/j.jag.2010.09.006>

661 Mason DC, Cobby DM, Horritt MS, Bates PD. 2003. Floodplain friction parameterization in
662 two-dimensional river flood models using vegetation heights derived from airborne scanning
663 laser altimetry. Hydrol Process. 17(9):1711–1732.

664 Mazzoleni M, Alfonso L, Chacon-Hurtado J, Solomatine D. 2015. Assimilating uncertain,
665 dynamic and intermittent streamflow observations in hydrological models. Adv Water Resour
666 [Internet]. 83(August):323–339.
667 <http://linkinghub.elsevier.com/retrieve/pii/S0309170815001517>

668 Mazzoleni M, Chacon-Hurtado J, Noh SJ, Seo D-J, Alfonso L, Solomatine D. 2018. Data
669 Assimilation in Hydrologic Routing: Impact of Model Error and Sensor Placement on Flood

670 Forecasting. *J Hydrol Eng* [Internet]. 23(6):04018018.
671 [https://ascelibrary.org/doi/pdf/10.1061/%28ASCE%29HE.1943-](https://ascelibrary.org/doi/pdf/10.1061/%28ASCE%29HE.1943-5584.0001656%0Ahttp://ascelibrary.org/doi/10.1061/%28ASCE%29HE.1943-5584.0001656)
672 [5584.0001656%0Ahttp://ascelibrary.org/doi/10.1061/%28ASCE%29HE.1943-5584.0001656](http://ascelibrary.org/doi/10.1061/%28ASCE%29HE.1943-5584.0001656)

673 McFeeters SK. 1996. The use of the Normalized Difference Water Index (NDWI) in the
674 delineation of open water features. *Int J Remote Sens*. 17(7):1425–1432.

675 McFeeters SK. 2013. Using the normalized difference water index (ndwi) within a
676 geographic information system to detect swimming pools for mosquito abatement: A
677 practical approach. *Remote Sens*. 5(7):3544–3561.

678 Mukherjee NR, Samuel C. 2016. Assessment of the temporal variations of surface water
679 bodies in and around Chennai using landsat imagery. *Indian J Sci Technol*. 9(18).

680 Mukolwe MM, Yan K, Di Baldassarre G, Solomatine DP. 2016. Testing new sources of
681 topographic data for flood propagation modelling under structural, parameter and observation
682 uncertainty. *Hydrol Sci J*. 61(9):1707–1715.

683 Nardi F, Cudennec C, Abrate T, Allouch C, Annis A, Assumpção T, Aubert AH, Bérod D,
684 Braccini AM, Buytaert W, et al. 2021. Citizens AND Hydrology (CANDHY):
685 conceptualizing a transdisciplinary framework for citizen science addressing hydrological
686 challenges. *Hydrol Sci J* [Internet]. 00(00):1–18.
687 <https://doi.org/10.1080/02626667.2020.1849707>

688 NLWRA NL and WRA. 2000. Australian Water Resource Assessment. [place unknown].

689 Pappenberger F, Beven K, Frodsham K, Romanowicz R, Matgen P. 2007. Grasping the
690 unavoidable subjectivity in calibration of flood inundation models: A vulnerability weighted
691 approach. *J Hydrol* [Internet]. [accessed 2014 Aug 11] 333(2–4):275–287.
692 <http://linkinghub.elsevier.com/retrieve/pii/S0022169406004318>

693 Pappenberger F, Beven K, Horritt M, Blazkova S. 2005. Uncertainty in the calibration of
694 effective roughness parameters in HEC-RAS using inundation and downstream level
695 observations. *J Hydrol* [Internet]. [accessed 2014 Jul 26] 302(1–4):46–69.
696 <http://linkinghub.elsevier.com/retrieve/pii/S0022169404003294>

697 Pappenberger F, Frodsham K, Beven KJ, Romanovicz R, Matgen P. 2007. Fuzzy set
698 approach to calibrating distributed flood inundation models using remote sensing
699 observations. *Hydrol Earth Syst Sci* [Internet]. 11(2):739–752. [http://www.hydrol-earth-syst-](http://www.hydrol-earth-syst-sci.net/11/739/2007/)
700 [sci.net/11/739/2007/](http://www.hydrol-earth-syst-sci.net/11/739/2007/)

701 Paul JD, Buytaert W, Allen S, Ballesteros-Cánovas JA, Bhusal J, Cieslik K, Clark J, Dugar S,
702 Hannah DM, Stoffel M, et al. 2018. Citizen science for hydrological risk reduction and
703 resilience building. *Wiley Interdiscip Rev Water*. 5(1):e1262.

704 Prestininzi P, Di Baldassarre G, Schumann G, Bates PD. 2011. Selecting the appropriate
705 hydraulic model structure using low-resolution satellite imagery. *Adv Water Resour*
706 [Internet]. 34(1):38–46. <http://dx.doi.org/10.1016/j.advwatres.2010.09.016>

707 Rogencamp G. 2004. Lower Clarence River Flood Study Review – Final Report: March
708 2004: Volume 1 of 2 Main Text. [place unknown].

709 Schnebele E, Cervone G, Waters N. 2014. Road assessment after flood events using non-
710 authoritative data. *Nat Hazards Earth Syst Sci* [Internet]. 14(4):1007–1015. [http://www.nat-](http://www.nat-hazards-earth-syst-sci.net/14/1007/2014/nhess-14-1007-2014.html)
711 [hazards-earth-syst-sci.net/14/1007/2014/nhess-14-1007-2014.html](http://www.nat-hazards-earth-syst-sci.net/14/1007/2014/nhess-14-1007-2014.html)

712 Schumann G, Matgen P, Hoffmann L, Hostache R, Pappenberger F, Pfister L. 2007. Deriving
713 distributed roughness values from satellite radar data for flood inundation modelling. *J*
714 *Hydrol* [Internet]. [accessed 2014 Aug 11] 344(1–2):96–111.
715 <http://linkinghub.elsevier.com/retrieve/pii/S0022169407003861>

716 Schumann G, Pappenberger F, Matgen P. 2008. Estimating uncertainty associated with water
717 stages from a single SAR image. *Adv Water Resour* [Internet]. [accessed 2014 Aug 8]
718 31(8):1038–1047. <http://linkinghub.elsevier.com/retrieve/pii/S0309170808000651>

719 See L. 2019. A review of citizen science and crowdsourcing in applications of pluvial
720 flooding. *Front Earth Sci.* 7(March):1–7.

721 See L, Fritz S, Dias E, Hendriks E, Mijling B, Snik F, Stammes P, Vescovi FD, Zeug G,
722 Mathieu PP, et al. 2016. Supporting earth-observation calibration and validation: A new
723 generation of tools for crowdsourcing and citizen science. *IEEE Geosci Remote Sens Mag.*
724 4(3):38–50.

725 Shaad K, Ninsalam Y, Padawangi R, Burlando P. 2016. Towards high resolution and cost-
726 effective terrain mapping for urban hydrodynamic modelling in densely settled river-
727 corridors. *Sustain Cities Soc* [Internet]. 20:168–179.
728 <http://dx.doi.org/10.1016/j.scs.2015.09.005>

729 Sinclair Knight Merz F, Roads and Traffic Authority of NSW TPS. 2011. Wells Crossing to
730 Iluka Road: upgrading the Pacific Highway: Tyndale to Maclean alternative alignment:
731 decision report. [place unknown].

732 Stephens E, Bates P. 2015. Assessing the reliability of probabilistic flood inundation model
733 predictions. *Hydrol Process* [Internet].:n/a-n/a. <http://doi.wiley.com/10.1002/hyp.10451>

734 Stephens E, Schumann G, Bates P. 2014. Problems with binary pattern measures for flood
735 model evaluation. *Hydrol Process.* 28(18):4928–4937.

736 Sunkara V, Purri M, Saux B Le, Adams J. 2020. Street to Cloud: Improving Flood Maps
737 With Crowdsourcing and Semantic Segmentation. In: *NeurIPS2020* [Internet]. [place
738 unknown]; p. 1–5. <http://arxiv.org/abs/2011.08010>

739 Tarpanelli A, Brocca L, Melone F, Moramarco T. 2013. Hydraulic modelling calibration in
740 small rivers by using coarse resolution synthetic aperture radar imagery. *Hydrol Process*.
741 27(9):1321–1330.

742 Tellman B, Lall U, Islam AKMS, Bhuyan MA. 2022. Regional Index Insurance Using
743 Satellite-Based Fractional Flooded Area. *Earth's Futur*. 10(3).

744 Wang Y, Ruan R, She Y, Yan M. 2011. Extraction of water information based on
745 RADARSAT SAR and Landsat ETM+. *Procedia Environ Sci* [Internet]. 10(PART C):2301–
746 2306. <http://dx.doi.org/10.1016/j.proenv.2011.09.359>

747 Wealands SR, Grayson RB, Walker JP. 2005. Quantitative comparison of spatial fields for
748 hydrological model assessment - Some promising approaches. *Adv Water Resour*. 28(1):15–
749 32.

750 Werner MGF, Hunter NM, Bates PD. 2005. Identifiability of distributed floodplain roughness
751 values in flood extent estimation. *J Hydrol* [Internet]. [accessed 2014 Aug 11] 314(1–4):139–
752 157. <http://linkinghub.elsevier.com/retrieve/pii/S0022169405001514>

753 Van Wesemael A, Landuyt L, Lievens H, Verhoest NEC. 2019. Improving flood inundation
754 forecasts through the assimilation of in situ floodplain water level measurements based on
755 alternative observation network configurations. *Adv Water Resour* [Internet].
756 130(January):229–243. <https://doi.org/10.1016/j.advwatres.2019.05.025>

757 Wing OEJ, Bates PD, Sampson CC, Smith AM, Johnson KA, Erickson TA. 2017. Validation
758 of a 30 m resolution flood hazard model of the conterminous United States. *Water Resour*
759 *Res*. 53(9):7968–7986.

760 Wood M, Hostache R, Neal J, Wagener T, Giustarini L, Chini M, Corato G, Matgen P, Bates
761 P. 2016. Calibration of channel depth and friction parameters in the LISFLOOD-FP hydraulic

762 model using medium-resolution SAR data and identifiability techniques. Hydrol Earth Syst
763 Sci. 20(12):4983–4997.

764 Ye W, Hansen DP, Jakeman AJ, Sharma P, Cooke R. 1997. Assessing the natural variability
765 of runoff: Clarence Basin catchments, NSW, Australia. Math Comput Simul [Internet]. 43(3–
766 6):251–260. [http://www.sciencedirect.com/science/article/B6V0T-3SP2CCR-](http://www.sciencedirect.com/science/article/B6V0T-3SP2CCR-3/2/2ab91a85f51787e7c9fa88de185219bc)
767 [3/2/2ab91a85f51787e7c9fa88de185219bc](http://www.sciencedirect.com/science/article/B6V0T-3SP2CCR-3/2/2ab91a85f51787e7c9fa88de185219bc)

768 Yu D, Yin J, Liu M. 2016. Validating city-scale surface water flood modelling using crowd-
769 sourced data. Environ Res Lett. 11:1748–9326.

770 Zhang X, Beeson P, Link R, Manowitz D, Izaurrealde RC, Sadeghi A, Thomson AM, Sahajpal
771 R, Srinivasan R, Arnold JG. 2013. Efficient multi-objective calibration of a computationally
772 intensive hydrologic model with parallel computing software in Python. Environ Model
773 Softw. 46:208–218.

774